Multi-Disciplinary Engineering Design Conference
Kate Gleason College of Engineering
Rochester Institute of Technology
Rochester, New York 14623

Project Number: 08501

DEVELOPMENT OF A ROLLER FUSER TEST BED

Arjun Sachdeva / Electrical Engineer **Nikhil Kaushal / Electrical Engineer**

Abdul Haleem Syed / Electrical Engineer

Daniel O' Connell / Mechanical Engineer **Nathan Po / Mechanical Engineer**

ABSTRACT

A roller fuser test bed was designed to emulate the fusing process of a printing system. Most laser printers and copiers in use today utilize the roller based fusing. The system facilitated complete user control over temperature and pressure application in the nip, and the number of pages printed per minute. User control and measurement of the aforementioned process parameters was exercised via an interface designed in LabView. The test bed was designed to be modular to give the user the ability to delve in to the experimental space in an effort to improve the operation of current laser printing systems.

Key Words: Fuser, nip width, Control, temperature, pressure, speed, image quality, dynamic model.

BACKGROUND

Fusing, the final step in the laser printing process comprises of bonding of toner powder on to print media via the application of heat and pressure. Laser based printing systems apply heat with aid of the top roller and pressure is applied by pressing down the top roller on to the bottom one. The small contact area formed between the two rollers when they are pressed together is referred to as the nip. The values of the process parameters inside the nip are critical as they play a major role in the final image quality. This field thus encompasses an area of further research and study and warrants the design and construction of a test system that replicates the working of actual fusing systems in use today while giving the user the ability to control and measure each process variable independently.

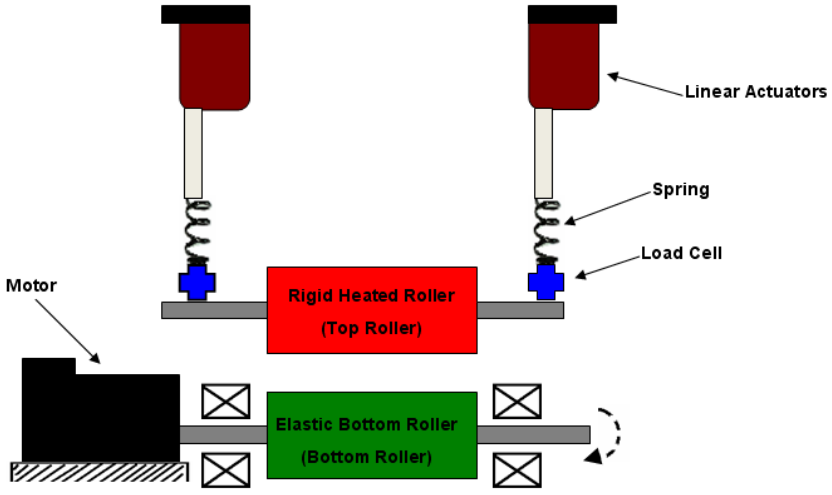

Figure 1: Roller Fuser Test Bed (RFTB)

This will allow the researcher to run experiments to determine an optimal set of parameter values to achieve the best possible image quality.

I. CUSTOMER NEEDS

The first task addressed by the team was to summarize the customer requirements to better understand the objectives of the project. To this end, brainstorming sessions usually followed by interview sessions with the customer were conducted. Customer needs were then summarized and ranked for importance on a scale of 1 (lowest) – 9 (highest) (Table 1).

Accuracy of the data measured and control of the process parameters obtained the highest rank because one of the main objectives behind the construction of the RFTB was improvement in image quality based on accurate control and measurement of process parameters. Modularity was also identified as a primary goal to give future research teams enough room for experimentation. The system's ability to emulate the operation of commonly used laser printers was also a high ranked requirement.

Ease of usability of the user interface was also deemed necessary since the test bed is not an automated system, and required interaction with the user. Other important needs included ability of the test bed to use the standard A.C. line (110V; 60 Hz) as its primary source of voltage. An emergency switch that when pressed may bring every subsystem to a stop, documentation detailing the operation of RFTB and low maintenance requirements were also required.

Table 1: Customer Needs

Customer Needs	Rank
Modularity	9
Simulation of the real world system	9
Accuracy	9
Controls and Measurement	9
Usability	3
Safety	3
Plug into standard wall outlet	3
Good functional user interface	9
Kill switch	3
Documentation (operators manual)	3
Maintenance	1

II. CONCEPT DEVELOPMENT

This phase of the project involved generation of ideas in order to achieve the customer needs listed in Table 1.The task of designing the RFTB was initiated by breaking down the RFTB system in to three major subsystems. These subsystems were created based on the process parameters that were defined as pressure and temperature in the nip, and speed of the rollers.

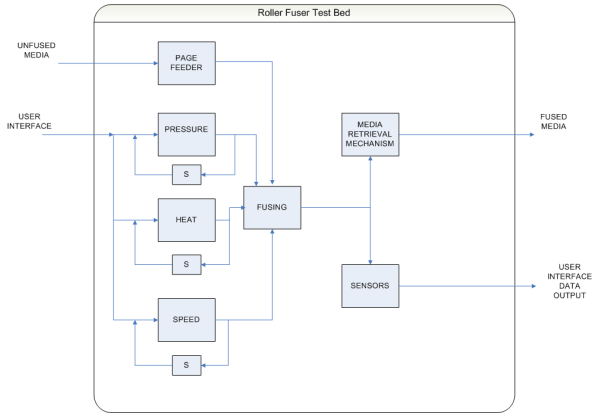

Figure 2: RFTB functional diagram

Requirement of a media feeding and retrieval mechanism was also adjudged during the concept development process. The use of additional sensors was also planned for in order to validate the data being measured. To better visualize the operation of the subsystems of the RFTB in conjunction with each other, an overall functional diagram was created (Figure 2). The functional diagram also highlighted the inputs and outputs to the system.

Extensive research about the ideas that were shortlisted in the brain storming sessions led to the finalization of solutions for the successful implementation of each sub-system (Table 2).

Table 2: Concept Development

System need to be addressed	Concept Development Sub-system solution
HEAT	Resistive Heating
PRESSURE	Actuators
SPEED	Electric Motor
FEED MEDIA	Feed Tray with friction
REMOVE MEDIA	Tray
SENSE TEMPERATURE	Infra Red
SENSE PRESSURE	Load Cells
USER INTEFACE	LabView

III. ENGINEERING SPECIFICATIONS

Specifics of the sub-system implementation solutions that were finalized in the concept development phase of

the project were determined. The target operating ranges for each subsystem are listed in table 3 below:

Table 3: Operating ranges for the major sub-systems

Nip Pressure	0-1.379 MN/m^2 (200 psi)
Pressure Sensing Accuracy	± 27.579 KN/m^2 (4 psi)
Temperature Control Range	0 – 523.15 K (250°C)
Temperature Sensing Accuracy	± 5.232 K (2.5 °C)
Speed Control Range	1 – 100 pgs/min (3-300 rpm)
Speed Sensing Accuracy	± 0.1pgs/min

IV. DYNAMIC MODELING

The task of modeling the proposed test bed (Figure 1) was broken down in to two parts: translational and rotational. The part of the test bed above the rollers was modeled as a translational system (Figures 3, 4) and the rollers (Figure 5) were modeled as a rotational system. The top roller acted as a link between the translational part and the rotational portion of the system.

A. TRANSLATIONAL SYSTEM

The translational system as discussed earlier consisted of linear actuators, springs, load cells and the top roller (Figure 3). The linear actuators used in the translational system were modeled as blocks of mass (M_1) with spring constant K_S (Figure 4).

A cup was used to hold the springs and the load cells together in the fixture. Physical properties of the cup were modeled in terms of blocks of mass M_2. Damping in the cup was approximated via a constant K_L. Lastly, the load cells were modeled with blocks of mass M_3 with the friction approximated by constant K_R.

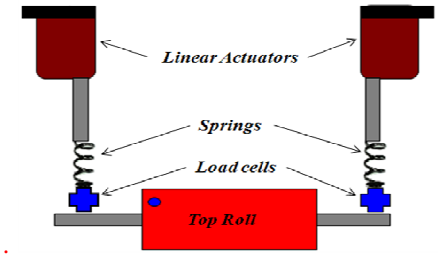

Figure 3: Translational model

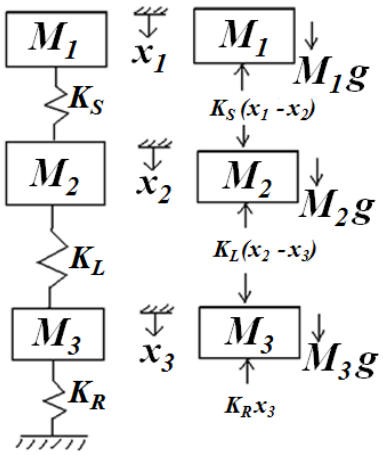

Figure 4: Physical representation of translational model

Linear motion of the top portion of the system was visualized with the help of its dynamic model ((1) – (3)). Overall linear displacement was broken down in to three sub displacements (x_1, x_2 and x_3; Figure 4) to provide the three displacements in the system. Force between M_1 and M_2, M_2 and M_3, and on M_3 was also clearly defined (Figure 4).

$$M_1\ddot{x}_1 = M_1 g - K_s(x_1 - x_2) \quad (1)$$

$$M_2\ddot{x}_2 = M_2 g + K_s(x_1 - x_2) - K_L(x_2 - x_3) \quad (2)$$

$$M_3\ddot{x}_3 = M_3 g + K_L(x_2 - x_3) - K_R(x_3) \quad (3)$$

B. ROTATIONAL SYSTEM

The rotational system consisted of the heated top roller and the bottom roller that was rotated with a DC motor (Figure 5). Moment of inertia of the motor, top roller and the bottom roller were coupled together in an equivalent moment of inertia (J_{eq}). Damping due to the motor (D_M), due to friction between top and bottom rolls and bearings (D_B) was represented by an equivalent damping factor D_{eq} (Figure 6).

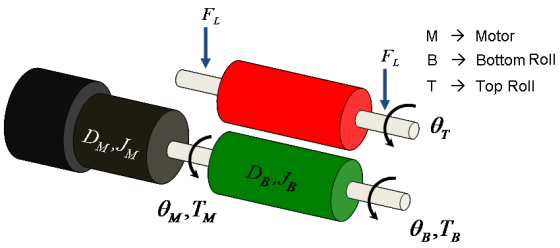

Figure 5: Rotational model

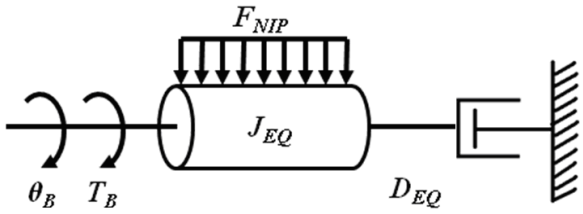

Figure 6: Physical representation of bottom model

Newton's laws were invoked to produce the mechanical relationship of the rotational half of the system (4).

$$T_{MOTOR} + J_{eq}\ddot{\theta}_B + D_{eq}\dot{\theta}_B + T_{LOAD} = 0 \quad (4)$$

T_{MOTOR} and T_{LOAD} represent the torque of the brushless DC motor and torque due to the force applied by the top roller on the bottom one.

Modeling of the DC brushless motor to obtain its torque as a function of the input AC line voltage was beyond the scope of this project. T_{MOTOR} once found can be used in equation 4 to determine the angular velocity of the bottom roller. T_{LOAD} was caused due to the force (F_L; Figure 7) due to the pushing action of the top roller on the bottom roller. Value for T_{LOAD} was calculated by visualizing the interaction of forces between the top and bottom rollers (Figure 7).

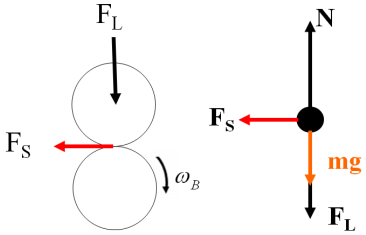

Figure 7: Illustration of interaction of forces between the top and bottom roller

Rotational force in the nip due to F_L was caused due to the action of linear force (F_S) also in the nip (Figure 7). Newton's concept of the sum of all forces acting at a point to be zero was utilized to represent the relationship between F_S, F_L and the reactionary force of the bottom roller (N) (5-6).

$$N = F_L + mg \quad (5)$$

F_S was represented in terms of the normal force (N) and the coefficient of static friction (μ_S) (6).

$$F_S = \mu_S N \quad (6)$$

The static friction coefficient (μ_S) was approximated as 0.4. Force between the two rollers (F_S) was calculated based on the maximum nip pressure (P_{NIP}) limit of the system (200 psi; Table 3). Inverse relationship between force and pressure was used to then obtain F_S from P_{NIP} (7-8). This conversion however also required information of the nip area (Figure 8) which was calculated based on measurements on the HP rollers' width (1 mm) and length (279.4 mm).

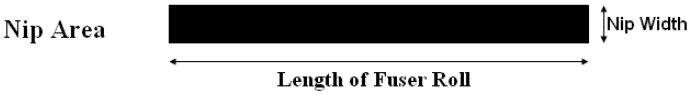

Figure 8: Nip area

$$F_S = P_{NIP} A_{NIP} \quad (7)$$

$$F_S = 1.379 * 10^6 * 279.4 * 10^{-6} = 385.3\,N \quad (8)$$

Maximum value of T_{LOAD} was then found by equating it to the product of the radius of the bottom roll and maximum force F_S (Figure 9; (9)). Radius of the bottom roll (r_B) was measured as 15 mm.

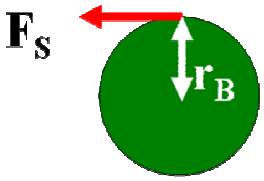

Figure 9: Visual representation of relationship between bottom roll torque, radius and frictional force (F_S)

$$T_{LOAD} = r_B F_S = 15 * 10^{-3} * 385.3 = 5.780\,\text{Nm} \quad (9)$$

Lastly, the angular velocity between the bottom and the top roll (Figure 10) were related as:

$$\frac{\omega_T}{\omega_B} = \frac{\dot{\theta}_T}{\dot{\theta}_B} = \frac{r_B}{r_T} \quad (10)$$

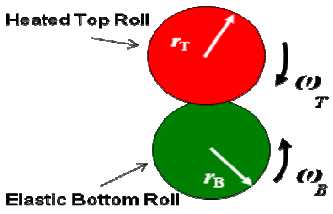

Figure 10: Top and bottom roll angular velocity relationship

PARAMETER ESTIMATION

Table 4 lists the parameters used in the modeling of the Roller Fuser Test Bed.

Values of spring constants for the load cell (K_L) were obtained to be 250 kpi [1].

Spring constant of the bottom roller (K_R) is a function of the material of the bottom roller. Elasticity of the material bears a direct relationship to the amount of pressure in the nip. Pressure variations in the nip are brought about due to deformation of the bottom roll due to the force applied to it by the top roll. The bottom roll is made of silicon rubber material with a modulus of elasticity in the range of 0.13 ksi (896.32 KN/m^2) to 0.848 ksi (5.847 MN/m^2).
Hooke's law was used to calculate the lower and upper value of the spring constant with a force equal to the upper and lower limits of the aforementioned elasticity range, and the area and width of the nip (11).

$$K_R = \frac{P_{NIP} A_{NIP}}{Nip\ width} \tag{11}$$

K_R was thus calculated to vary between 250.07 N/m and 1.631 MN/m.

Spring constant of the spring (K_S) was also calculated using Hooke's law. The force under consideration for K_S was F_S that was caused by the loading on the system ((8); Figure 7).
Since the force (F_S) acting in the nip was due to the combined loading of two linear actuators on two springs, only half of F_S acting on one spring was used to calculate the value of the spring constant (K_S). The springs were assumed to have a maximum displacement (x) of 3 inches (76.2 mm) (Figure 11; (12)).

$$K_S = \frac{0.5 * F_S}{0.0762} = 2.528 \frac{KN}{m} \tag{12}$$

Table 4: Parameters used to model the RFTB

D_M	Motor damping
D_B	Bottom roll's damping
$D_{eq} = D_M + D_B$	Equivalent Damping
F_L	Loading from the linear actuators
F_{NIP}	Nip Loading
K_S	Spring Constant for the spring
K_L	Spring Constant for the Load Cell
K_R	Spring Constant for the Roller
M_1	Mass of Springs
M_2	Mass of the cup that holds the springs and the load cell
M_3	Mass of Load Cell
T_{MOTOR}	Brushless DC motor torque
T_{LOAD}	Frictional torque between rollers
J_M	Motor's moment of inertia
J_B	Bottom roll's moment of inertia
$J_{eq} = J_M + J_B$	Equivalent moment of inertia
θ_B	Angular displacement of bottom roller
$\dot{\theta}_B$	Angular velocity of bottom roller
$\ddot{\theta}_B$	Angular acceleration of bottom roller
K	Electromagnetic constant
r_B	Radius of the roller

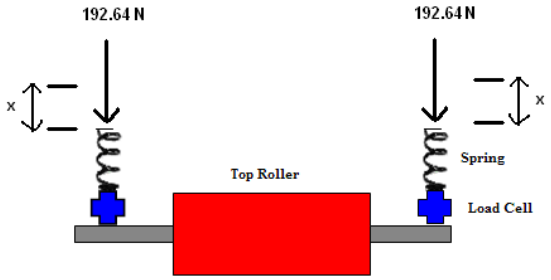

Figure 11: Description of dividing the force between the two springs

V. PARTS SELECTION

Products for each sub-system were selected to ensure the operation of the entire system in the defined operating ranges. Interaction between various sub-systems was also considered in the selection process.

- PRESSURE SUB-SYSTEM

Linear actuators were used to load the ends of the top roller which translated in to pressure in the nip. Actuators manufactured by Firgelli Automation that have a maximum load capacity of 891.8 N (100 lbf) were selected. Two linear actuators (one on each side; Figure 3) were used to meet the desired pressure operation range (Table 3). Ability of the actuators to extend out by 6 inches further aided pressure application. The force needed to create a maximum pressure of 200 psi in the nip was calculated with the force and pressure relationship (7-8).
The linear actuators were powered and controlled using an external driver and controller board. Position of the linear actuators was reported via a potentiometer analog voltage reading. The feedback voltage was read in to the controller boards which employed a PID control mechanism to ensure proper positioning of the actuators. Accurate position control of the actuator guaranteed accurate control of pressure in the nip. Position of the actuators to apply specific force values in the nip was set via LabView.
Net force in the nip (F_{NIP}; Figure 6) was measured with the aid of load cells manufactured by Omega Engineering. Each load cell had the ability to measure a force up to 1.784 KN (200 lbf).

- SPEED SUB-SYSTEM

A speed control system manufactured by Oriental Motors that consists of a brushless DC motor with an optical encoder and a PID controller was used to rotate the bottom roller and control the number of pages fused per minute (Figure 1). Rated torque of the motor was taken in to careful consideration to ensure the operation of the motor even under maximum loading. Torque required to rotate the bottom roller at a pressure of 200 psi was calculated to be 20.986 lb-in (2.371 Nm) (13-14).

$$T_{MOTOR\max} = r_B \mu_S N = r_B \mu_S (F_{L(MAX)} + mg) \quad (13)$$

$$T_{MOTOR\max} = 0.015 * 0.4(1.379 * 279.4 + 9.8) = 2.371\,Nm \quad (14)$$

The rated torque of the selected brushless DC motor was 46 lb-inches (5.197 N-m) which met the desired peak torque. Number of revolutions of the bottom roll with a radius (r_B) of 1.5 cm to traverse the length of an 11 inch (279.4 mm) long page was calculated to be 3 as shown in equation (15).

$$Revolutions = \frac{0.2794}{2 * 3.14 * 0.015} \approx 3 \quad (15)$$

Thus, in order to fuse a maximum of 100 pages per minute, the desired motor was required to have 300 revolutions per minute. Since the selected motor had a maximum rpm of 300, the 100 pages per minute requirement was met.
The PID controller of the motor took care of the angular displacement of the motor which was kept track of and set using LabView. The optical encoder that produced 500 pulses for each revolution of the motor was also one of the reasons for its selection since a feedback mechanism to confirm the set speed was desired. Both the controller and the DC motor worked on standard line voltage (110-115 VAC) which is readily available.

- TEMPERATURE SUB-SYSTEM

An Infrared sensor manufactured by Raytek was used in order to measure the temperature in the nip. The selected sensor had a wide sensing range that met the desired sensing range of 0 – 250 °C (Table 3). Since the worst case approximation of the nip width was 1 mm. Thus a sensor that could measure temperature accurately over small areas was required. The selected sensor has the capability of measuring temperature of a circular spot of diameter 1.1 mm (0.04 inches) from a distance of 76 mm (3 inches) from it. This gave the ability to measure the temperature in the nip relatively accurately as compared to other explored options. Since the emissivity of the sensor could be set anywhere in the range of 0.1 to 1.150, it was a good choice as it added to the modularity of the system because the same sensor could be used to measure temperature of different roller and paper materials. The sensor also had a vast spectral response of 8 – 14 µm which further added to the RFTB's modularity. Another key feature of the sensor was the presence of laser targeting which was helpful in determining the target spot whose temperature is to be measured. Lastly, a fast response time was desirable as at high pages per minute speeds, temperature changes will be required to be noticed expeditiously. The chosen sensor had a response time of 120 ms which was much faster than the other IR and thermocouple/ thermistor based sensors that were explored.
The measured temperature could be viewed either on the LCD screen of the sensor or via LabView by tapping in to the sensor's analog current outputs.

To control the temperature in the nip, an external temperature controller manufactured by Oven Industries was purchased. The selected controller board was compatible with the existent fuser assembly

thermistors. The range of temperatures that can be applied via the temperature controller primarily depended on the feedback thermistor. This added to the modularity of the system as a higher temperature range can be applied by upgrading to a different feedback sensor. Response of the heating element was shaped via PID control on the controller board.

VI. RESULTS AND CONCLUSIONS

All the subsystems described in the previous sections were controlled and monitored using a common user interface in LabView. Experiments were run to check if the end goal of fusing an unfused image through the RFTB was achieved.

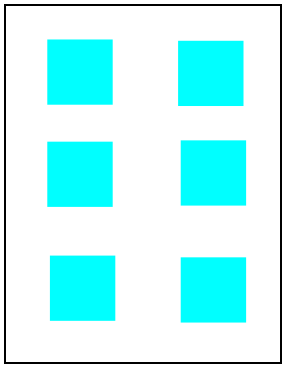

Figure 12: Unfused print pattern

An array of unfused toner patches (Figure 12) was passed through the RFTB at different nip temperature, speed and pressure settings. Specifically, five different parameter combinations were tried for the fusing process (Table 5).

Table 5: Experiment parameter settings

Trial #	Total Loading Force (lbs)	Temperature (°C)	Pages per minute
1	20	120	7
2	20	160	7
3	20	180	7
4	20	180	12
5	20	180	25

The loading force was kept constant for all trials. The nip temperature was increased from 120 °C to 180 °C in increments of 40 °C at a rate of 7 pages per minute. 180 °C was observed to yield optimum fusing. The temperature was thus fixed at 180 °C and the page fusing rate was varied from 7 pages per minute to 12, and finally to 25 pages per minute.

In addition to visual evaluation of fused toner, the tape test was used to check the degree of toner fixing achieved. In this test, a piece of scotch tape is pasted on to the fused toner and then peeled off. The greater the quantity of toner that sticks to the tape, the lower is the degree of fixing that is achieved.

Best fusing was achieved during the third trial of the experiment (Table 5).

VII. RECOMMENDATIONS FOR FUTURE WORK

For future improvements higher precision linear actuators are recommended to be used with a digital feedback to ensure a more accurate position and speed control. This will enable more control over the pressure being applied in the nip. Another way to increase position control would be to purchase linear actuator controllers with high resolution to incorporate smaller incremental steps while altering the position. Nip pressure will thus be more controllable. An improved mechanical system to guide the linear actuator shafts should replace the present setup.

Temperature sensing using the IR sensor can be implemented via a RS-485 interface. This will make the process of reading the measured temperature in to LabView digital and will thus remove the need for careful setup of the temperature measurement range.
Temperature control system can be integrated in to the main LabView visual interface. This will further simplify the use of the RFTB as an additional program will not have to be run to set the desired nip temperature. The current temperature control system uses feedback from a sub-thermistor that is in direct contact with the top roller's ceramic strip. Control of nip temperature can also be implemented using feedback from the main thermistor that sits on the top roller's sleeve.

Lastly, a kill switch can be added to sever the connection of the RFTB to sources of AC and DC power in case of an emergency situation.

ACKNOWLEDGMENTS

The roller fuser test bed team would like to thank all those who helped make the test bed possible. We would like to thank our sponsor Hewlett Packard.

Special thanks to our faculty guide Dr. Esterman.

We would also like to thank Dr. Arney, Dr. Cockburn, Dr. Farnand, and Alvaro Rojas for their support and guidance.

REFERENCES

[1] www.matweb.com